

PACS numbers: 42.55.Rz; 42.60.Jf
DOI: 10.1070/QE2005v035n04ABEH003419

Compact neodymium phosphate glass laser emitting 100-J, 100-GW pulses for pumping a parametric amplifier of chirped pulses

A.K. Potemkin, E.V. Katin, A.V. Kirsanov, G.A. Luchinin, A.N. Mal'shakov, M.A. Mart'yanov, A.Z. Matveev, O.V. Palashov, E.A. Khazanov, A.A. Shaikin

***Abstract*. A five-stage neodymium phosphate glass amplifier producing 1 – 1.5-ns radiation pulses of energy up to 110 J is described. The use of a multistage spatial filter based on an aperture line provides efficient extraction of the stored energy. The exit aperture filling factor is 0.65 and the output radiation divergence is equal to three times the diffraction-limited divergence. The energy efficiency of radiation conversion to the second harmonic is 60 %. The amplifier is intended for pumping a chirped-pulse optical parametric amplifier.**

Keywords: *neodymium glass lasers, Nd : YLF lasers, aperture filling factor, spatial filters.*

1. Introduction

In [1], a new high-power femtosecond laser design based on optical parametric amplifiers (OPAs) of the pulses chirped in DKDP crystals is described. The first OPA stages were pumped by the 527-nm second harmonic of a repetitively pulsed Nd : YLF laser. The use of one more OPA stage in this laser may provide output pulses up to 100 TW. Pumping this stage requires the second harmonic of a pulsed neodymium phosphate glass laser with a wavelength coinciding with the Nd : YLF-laser wavelength. The energy of the second harmonic radiation pulse should be no less than 50 J for a pulse duration of 1 – 2 ns and a radiation divergence no greater than 100 μrad. The spectral width $\Delta\nu$ should correspond to the pulse duration τ ($\Delta\nu = 2/(\pi c\tau) < 0.01 - 0.02$ cm^{-1}) and filling factor of the laser exit aperture F should be equal to 0.5 – 0.7. The real coefficient of radiation conversion to the second harmonic usually does not exceed 50 % – 70 %, and therefore the energy of the fundamental harmonic at the laser output should be no less than 100 J.

Laser setups with such parameters and an output energy of 0.1 – 10 kJ were first constructed in the mid-1970s (Shiva, Omega, etc.) [2, 3]. However, they are characterised by the great complexity of design and maintenance. More recent papers [4, 5] reported the development of less cumbersome lasers with similar output parameters, which was due to the employment of high-efficiency phosphate glass rod amplifiers [6 – 8], the development of techniques for the formation of a transverse spatial structure with a large filling factor [9, 10], and the methods for suppressing small-scale self-focusing [4, 9, 11]. Note that lasers similar to those described in Ref. [4] are still rather cumbersome, expensive, and complex in maintenance, and therefore the use of additional chirped-pulse amplification stages is undoubtedly of considerable interest.

The laser for pumping an OPA is an important though not the central part of a femtosecond laser system. That is why it should be simple in maintenance, reliable, and relatively compact (it is desirable to accommodate it on a single optical table). It is precisely this kind of laser that is considered in this work.

Figure 1 shows the optical layout of the system for pumping all OPAs (OPA I – OPA III) of a 100-TW femtosecond laser. It contains repetitively pulsed Nd : YLF laser (*1*), a scheme which forms spatial beam structure (*3 – 8*), five-stage neodymium phosphate glass laser amplifier (*9*, *15*, *17*, *19*, *21*), and second-harmonic generator (*22*). The five-stage amplifier comprises four single-pass amplifiers (*9*, *17*, *19*, *21*) and one two-pass amplifier (*15*) as well as transport telescopes (*14*, *18*, *20*). To avoid self-excitation of the amplifier, Faraday isolator (*10*, *11*) is used. The main part of the amplifier is accommodated on a honeycomb optical table of size 350 × 120 cm. Only final amplifier (*21*) and second harmonic generator (*22*) are located exterior to the table.

2. Repetitively pulsed Nd : YLF laser

The Nd : YLF laser with a repetition rate of 2 Hz (Fig. 2) was employed both for the successive pumping of the first two OPA stages [1] and to pump the neodymium glass laser (Fig. 1).That is why the Nd : YLF laser has two outputs: the main output, with the energy of the fundamental harmonic of 2 J and the energy of the second harmonic of 1 J, and the auxiliary output, with the fundamental harmonic energy of 200 mJ.

The ~0.5-m long resonator of the master oscillator is formed by two highly reflecting mirrors M1 and M2. A polariser P1 and a quarter-wave plate QWP1 provide polarised radiation extraction. The Nd : YLF crystal (5-mm diameter, 75-mm long active region, 1 % Nd ion concentration) is accommodated in a two-flashlamp laser

A.K. Potemkin, E.V. Katin, A.V. Kirsanov, G.A. Luchinin, A.N. Mal'shakov, M.A. Mart'yanov, A.Z. Matveev, O.V. Palashov, E.A. Khazanov, A.A. Shaikin Institute of Applied Physics, Russian Academy of Sciences, ul. Ul'yanova 46, 603950 Nizhnii Novgorod, Russia; web-site: www.sci-nnov.ru/science/science/appl.new/; e-mail: ptmk@appl.sci-nnov.ru

Received 20 December 2004
Kvantovaya Elektronika **35** (4) 302 – 310 (2005)
Translated by E.N. Ragozin

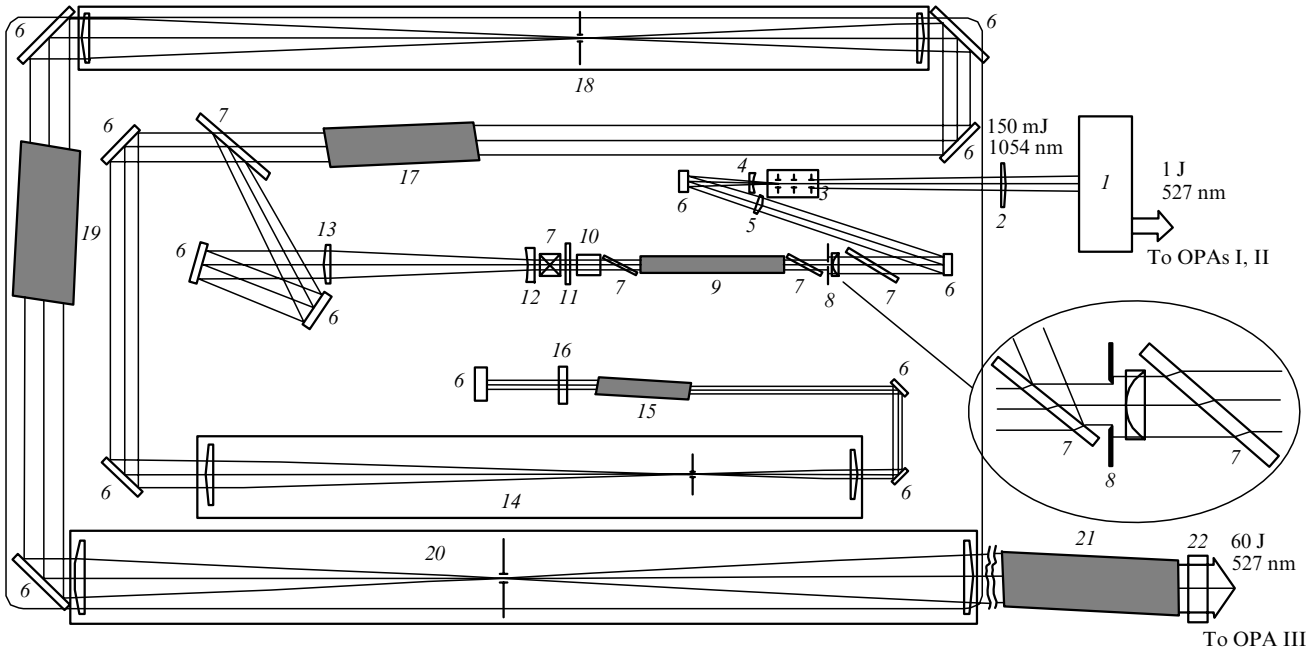

Figure 1. Scheme of the pump system: (*1*) Nd : YLF laser (see Fig. 2); (*2*) lens with a focal distance $f = 1 - 3$ m; (*3*) aperture line; (*4*) lens with $f = -18.5$ cm; (*5*) lens with $f = 39$ cm; (*6*) highly reflecting mirror; (*7*) polarisers; (*8*) apodising screen; (*9*) amplifier with an active element measuring $\varnothing 1 \times 25$ cm; (*10*) Faraday rotator; (*11*) $\lambda/2$ plate; (*12*), (*13*) Galilean telescope with a 6-fold magnification; (*14*) Keplerian telescope with a 3-fold magnification; (*15*) amplifier with an active element measuring $\varnothing 2 \times 12$ cm; (*16*) $\lambda/4$ plate; (*17*) amplifier with an active element measuring $\varnothing 6 \times 25$ cm; (*18*) Keplerian telescope with a 1.42-fold magnification; (*19*) amplifier with an active element measuring $\varnothing 8.5 \times 25$ cm; (*20*) Keplerian telescope with a 1.17-fold magnification; (*21*) amplifier with an active element measuring $\varnothing 10 \times 25$ cm; (*22*) second harmonic generator.

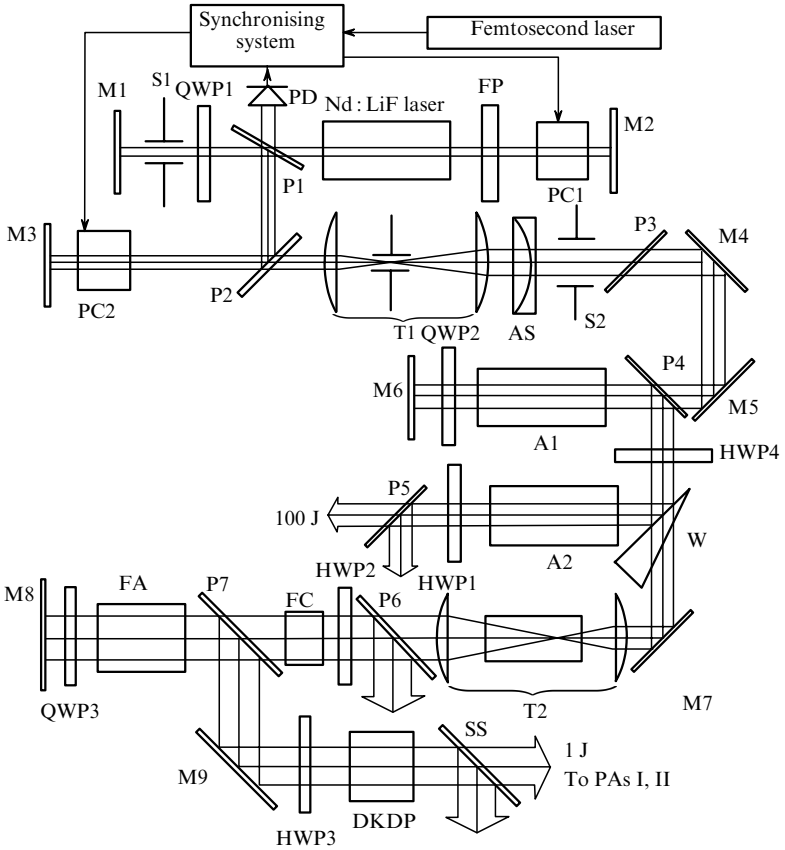

Figure 2. Scheme of the repetitively pulsed Nd : YLF laser: (M1) – (M9) mirrors; (S1) pin hole; (QWP1) – (QWP3) quarter-wave plates; (P1) – (P7) polarisers; (PD) photodiode; (FP) Fabry – Perot etalon; (PC1), (PC2) Pockels cells; (T1), (T2) telescopes; (AS) apodising screen; (S2) beam-limiting aperture; (A1), (A2) preamplifiers; (HWP1) – (HWP4) half-wave plates; (FC) Faraday cell; (FA) final amplifier; (DKDP) frequency doubling crystal; (SS) spectrum splitter; (W) glass wedge.

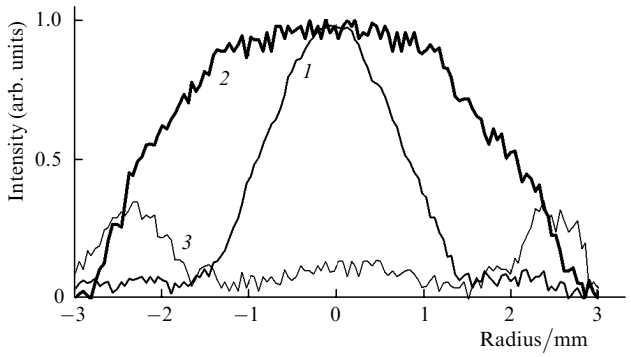

Figure 3. Intensity distributions of the beams after the master oscillator (*1*) and in front of preamplifier A1 (*2*) as well as of the beam reflected from polariser P3 (3).

head with a diffuse reflector. The crystal and the flashlamps are sequentially cooled with distilled water. An aperture A1 1.7 mm in diameter provides selection of transverse modes. The transverse near-field beam profile is shown in Fig. 3 [curve (*1*)]. The aperture filling factor

$$F = \frac{2\pi}{I_{\max}\pi R^2}\int_0^R I(r)r\mathrm{d}r,$$

where R and I are the aperture radius and the beam intensity, was equal to 0.28.

Longitudinal mode selection was performed with two Fabry–Perot air etalons with bases of 12 and 1 mm. An intracavity Pockels cell PC1 and its triggering photodiode PD provided a Q-switching regime [12, 13] with a giant-pulse duration of 15–20 ns and an energy of 8–10 mJ. For the parametric interaction to be efficient, the pump pulse duration should be 1–2 ns. The time jitter (random uncontrollable shift of the pulses of one laser relative to the other) of pump laser pulses and the pulse being amplified should therefore be within 100 ps [14]. This requirement was fulfilled with the help of an extracavity Pockels cell PC2 (Fig. 2), which clips an optical pulse (Fig. 4) with an energy of ~1 mJ [12].

After a four-fold magnifying telescope T1 with a spatial filter, the beam arrives at an apodising screen AS, a beam-limiting aperture A2, and a polariser P3, which provide a transverse beam intensity distribution close to the super-Gaussian distribution [15]. The apodising screen is a spherical plano-convex lens made of crystal quartz with its optical axis oriented at an angle of 45° to the direction of radiation polarisation. The lens thickness and the radius of curvature are so selected that the on-axis phase shift is equal to 2π and the phase shift is equal π some distance r_d from the axis. Therefore, the transmittance of the soft aperture is

$$T_a = \cos^2\left(\frac{\pi}{2}\frac{r^2}{r_d^2}\right). \quad (1)$$

To compensate for the divergence, the crystal quartz lens was put in optical contact with a lens of fused silica. After it, the beam passes through a beam-limiting aperture A2 with a radius r_d. The value of r_d was matched with the radius of the active element (AE) of the preamplifier and was equal to 2.7 mm. The beam profile ($F = 0.45$) at the input of the preamplifier A1 is shown in Fig. 3 [curve (*2*)].

The small-signal gain G_0 of the preamplifier A1 is ~25 – 30 per pass (Fig. 5). The Nd:YLF crystal (6-mm diameter, 60-mm long active region, 1 % Nd concentration) was cut in such a way that the angle between the optical axis and the wave vector was ~5°. On the one hand, this ensures efficient amplification of orthogonally polarised waves in both passages, and on the other hand, significantly suppresses the thermally induced birefringence and the depolarisation it induces [16].

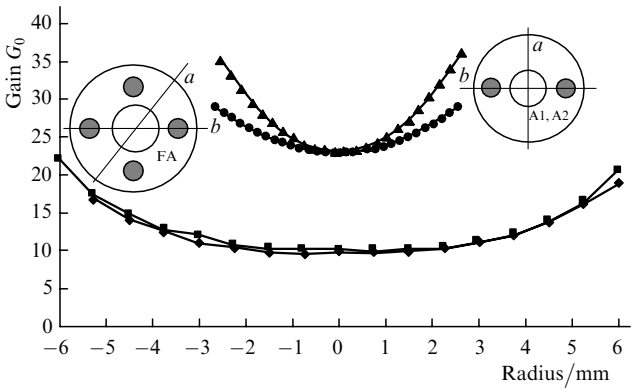

Figure 5. Transverse distributions of the small-signal gain G_0 in preamplifiers transversely to (●, *a* axis) and lengthwise of (▲, *b* axis) the direction of flashlamp arrangement and in the final amplifier lengthwise of the direction of flashlamp arrangement (■, *b* axis) and at an angle of 45° to this direction (◆, *a* axis).

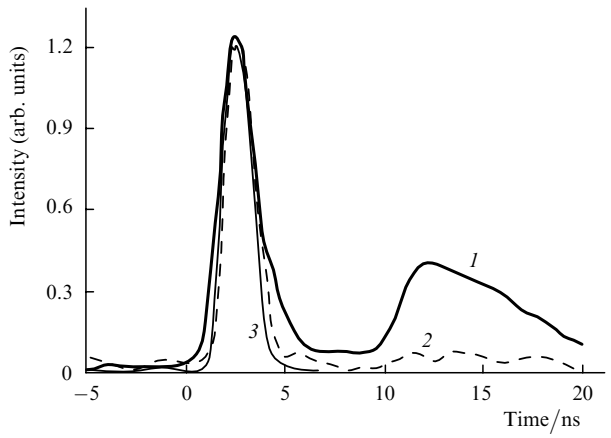

Figure 4. Oscilloscope traces of the pulses after the master oscillator (*1*), the final amplifier (*2*), and the frequency doubler (*3*).

After the second passage through A1, the pulse with an energy of ~70 mJ is directed to a beamsplitter glass wedge W by a polariser P4. The wedge deflected 10 % of the radiation energy to preamplifier A2 with a polarisation attenuator (HWP1 and P5), after which the energy at the auxiliary output of the Nd:YLF laser could be varied between 5 and 200 mJ without changing spatiotemporal characteristics.

A mirror M7 directs the beam to a magnifying telescope T2 with a vacuum cell to avoid the optical air breakdown and then to the two-pass final amplifier FA via a Faraday isolator. The Nd:YLF crystal (15-mm diameter, 90-mm long active region, 1 % Nd concentration) is accommodated in our specially designed four-flashlamp quantron (INP-5/90 flashlamps with a total electric energy of 400 J) with successive cooling of the AE and the flashlamps inside

the diffuse reflector. The small-signal gain measurement data are presented in Fig. 5.

Due to a quarter-wave plate QWP3, the vertically polarised useful radiation is reflected by a polariser P7. The depolarised part of radiation (less than 1 %) passes through the polariser P7 and then through the Faraday rotator to be removed from the setup by a polariser P6. Due to amplification saturation, the pulse duration becomes somewhat shorter and the contrast ratio between the main pulse and its following satellite [14] increases (Fig. 4). Furthermore, the saturation and the radial gain nonuniformity of A1 and FA (Fig. 5) lead to an increase in the filling factor F up to 0.75.

Conventional thin-film polarisers typically possess a vertical-polarisation transmittance of $\sim 10^{-3}$. This is insufficient to provide the efficient decoupling of FA and A1. That is why the substrate of the polariser P7 was coated on both sides, which lowered the vertical-polarisation transmittance to 10^{-6}. The energy of the pulse reflected from the polariser P7 is equal to ~ 2 J, the divergence is no greater than three-times the diffraction limit.

A DKDP crystal with a type-II interaction is employed to convert the radiation to the second harmonic. The second harmonic radiation (1-J energy, 1.3 – 1.7-ns duration for an 0.7 aperture filling factor) was separated with a spectrum splitter SS and directed to the first OPA stages [1].

3. Formation of spatial beam structure

Like in the Nd : YLF laser, in glass amplifiers (Fig. 1) the aperture filling factor F increases due to amplification saturation and the radial dependence of the gain. To maximise the F value at the laser output it should be optimised at the input. For this purpose, aperture line (*3*) (see Fig. 1) is employed in our work. Lens (*2*) focuses the beam to the input of spatial filter (*3*), which consists of three sequentially located apertures of diameter D equally spaced at a distance L. The focal distance of lens (*2*) is so selected that the diameter of the first dark ring at the entrance aperture is equal to $1.1D$.

Aperture lines with equal Fresnel numbers $N_F = D^2/(4\lambda L)$ possess similar selection properties. However, because of the plasma plume emerging at the edges of the apertures for some pulse energy W_{max} there occurs beam 'closure' by the plasma, the 'closure' rate being inversely proportional to the square root of the atomic number of the aperture material [2, 17]. By increasing D and L with retention of N_F and by optimising the material of the aperture, it is possible to increase W_{max}. Figure 6 shows the dependences of the output radiation energy behind filter (*3*) on the input energy, which were obtained for apertures made of molybdenum ($D_1 = 0.4$ mm, $L_1 = 11$ cm) and tantalum ($D_2 = 0.9$ mm, $L_2 = 33$ cm). The Fresnel numbers of the two aperture lines differ by less than a factor of two, and the highest energies transmitted by the filters differ 23-fold. The oscilloscope traces shown in Fig. 6 demonstrate the aperture 'closure' process for a high input energy. The measured pulsed response of the photodiode – cable – oscilloscope system was 250 ps.

The radiation is then directed to Galilean telescope (*4*), (*5*) and apodising screen (*8*). Its design was described in the previous Section. The radial distribution of light intensity at the apodising screen input is close to the far-field diffraction pattern produced by a round opening – the Airy distribution

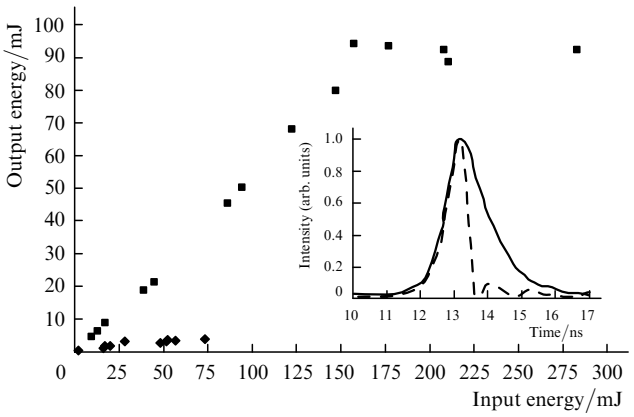

Figure 6. Transmission of pulses with $\tau = 1.5$ ns by an aperture line of molybdenum (◆, $D_1 = 0.4$ mm, $L_1 = 11$ cm) or tantalum (■, $D_2 = 0.9$ mm, $L_2 = 33$ cm). The oscilloscope traces in the inset correspond to the regimes of total (solid curve) and partial (dashed curve) pulse transmission by the aperture line.

with the radius of the first dark ring r_a – and remains invariable even for a severe pulse 'chopping'. When $r_d = r_a$, i.e. the zeroes of the Airy distribution coincide with the zeroes of the transmission coefficient of apodising screen (*1*), the aperture filling factor at its output is $F_d = 0.198$. When $r_d \ll r_a$, $F_d = 0.5$. Therefore, by changing the magnification of telescope (*4*), (*5*) it is possible to obtain any F_d in the 0.2 – 0.5 interval. We employed a telescope with a 2.3-fold magnification and filter (*3*) with $D_2 = 0.9$ mm and $L_2 = 33$ cm. In this case, $F_d = 0.45$ and the intensity distribution at the output of apodising screen (*8*) is shown in Fig. 7b. As shown below, the coefficient F will increase with amplification, which will permit a rather efficient use of the energy stored in the amplifiers.

To verify the selective properties of the aperture line, we changed the direction of the beam ($\pm 5 \times 10^{-4}$ rad) incident on lens (*2*) and the radius of curvature of its wave front (from -2 to $+3$ m). In doing this we kept track of the changes in beam direction and its near-field pattern. For filter (*3*) with $D_1 = 0.4$ mm and $L_1 = 11$ cm, the input beam deflection did not change the direction of the outgoing radiation. For filter (*3*) with $D_2 = 0.9$ mm and $L_2 = 33$ cm, the output beam deflection angle was five times smaller than the input beam deflection angle and the radius of curvature of the output beam was 50 times smaller than the radius of curvature of the input beam. The near-field transverse intensity distribution pattern (Fig. 7b) did not change under the above deviations.

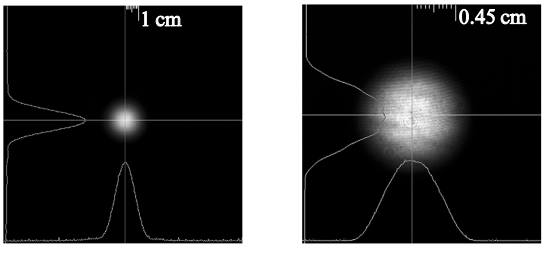

Figure 7. Transverse intensity distributions at the output of the second stage of the aperture line (a) and at the input to amplifier (*9*) (Fig. 1) (b).

4. Five-stage laser amplifier

To achieve the limiting light intensity at each amplifier stage requires controlling small-scale self-focusing (SSF). It is commonly characterised by the B-integral

$$B = \frac{8\pi^2 n_2}{\lambda c n}\int_0^l I(z)\mathrm{d}z, \qquad (2)$$

where n and n_2 are the linear and nonlinear refractive indices of the material of a medium; l is the length of the medium [18]. The main contribution to the integral B is made by a short length at the AE output, because the intensity I increases during the propagation of radiation through the AE. That is why increasing the gain G leads to a decrease in B and, hence, to an increase in the output intensity without an increase in the radiation divergence. Of the possible versions of laser heads, the highest gain G is provided by 'densely packed' quantrons with a Kersil reflector [6, 7], which we mostly employed (Table 1). The one exception was provided by the first amplifier (since its contribution to the integral B is small), which incorporates a four-ellipse specular reflector. Table 1 gives the integral increments ΔB at each amplification stage. We assumed that $n_2 = 1.07 \times 10^{-13}$ esu for the KGSS 1621 phosphate glass [19], $n_2 = 1.16 \times 10^{-13}$ esu for the K8 optical glass [20], and $n_2 = 1.93 \times 10^{-13}$ esu for the MOS-04 magneto-optical glass [20]. When calculating ΔB in the AEs we took into account the amplification saturation by using the Frantz–Nodvik formula [21]. The neodymium ion concentration was selected in such a way as to minimise the radial variation of G [22]. Measurements of the radial dependence of the gain $\alpha = (\ln G)/L_a$ (where L_a is the AE length) showed that it is parabolic. For the amplifier 10 cm in diameter, the increase in α at the edge of the AE amounts to 20 % compared to its centre and to less than 10 % for the remaining amplifiers.

The FWHM of the flashlamp light pulse is $\tau_{1/2} = 400 - 500$ μs. Figure 8 shows the dependence $f_x = W_e/W_x$ for the amplifier 2 cm in diameter, where f_x is the discharge energy W_e of the pump flashlamps normalised to the flashlamp damage energy W_x determined from the expression

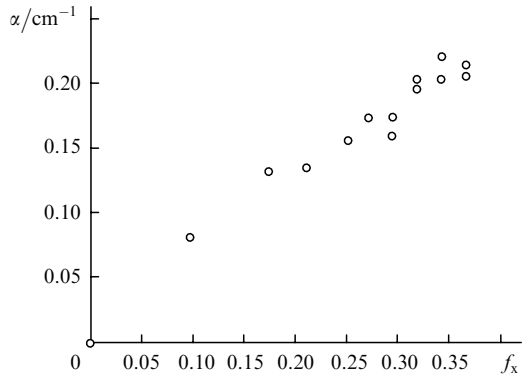

Figure 8. Gain $\alpha = (\ln G)/L_a$ as a function of specific flashlamp load for amplifier (*15*) (Fig. 1). The AE measures 2 cm in diameter and 12 cm in length.

$$W_x = 22000 L_f d\left(\frac{\tau_{1/2}}{2}\right)^{1/2},$$

where L_f and d are the interelectrode distance and the internal diameter of the flashlamp tube in centimetres; $\tau_{1/2}$ is the FWHM of the flashlamp discharge pulse in seconds [23]. The parameter f_x determines the number of flashes (the lifetime) N_e of the lamps according to an approximate empirical law: $N_e = f_x^{-11}$ [22, 23]. For the maximum value $f_x = 0.37$ presented in Fig. 8, $N_e = 6 \times 10^4$. A part of the radiation energy passes by an AE and returns to the flashlamps again, with the effect that they overheat and f_x increases to 0.5 [22]; as this takes place, $N_e = 2000$. This value of f_x may be thought of as being acceptable for the operation of a setup at this output energy level.

An important laser parameter is the pulse repetition rate. It is determined by the thermal relaxation time of the amplifier with the largest 10-cm aperture. To determine this time, we measured the dynamics of depolarisation degree γ in AEs in crossed polarisers. For a flashlamp load close to the limiting one, the γ value for an AE 6 cm in diameter 17 minutes after the discharge exceeds the degree of 'cool' depolarisation by no more than a factor of two. This time was adopted as the minimal interval between the shots; for other amplifiers it was scaled in proportion to the square of diameter.

Table 1. Parameters of neodymium glass amplifiers.

Amplifier (label in Fig. 1)	(*9*)	(*15*)		(*17*)	(*19*)	(*21*)
AE diameter/mm	10	20		60	85	100
AE length/cm	25	12		25	25	25
Glass type	GLS 22P	KGSS 1621-13		KGSS 1621-06	KGSS 1621-04	KGSS 1621-04
Nd ion density/10^{20} cm^{-3}	2.0	0.92		0.56	0.29	0.33
Reflector type	specular	diffuse		diffuse	diffuse	diffuse
Flashlamp type	IFP-5000	IFP-1200		IFP-8000	IFP-8000	IFP-8000
Number of flashlamps	4	12		12	16	18
Electric energy W_e/kJ	10.5	7.7		40	50	56
Small-signal gain G_0	300	14		6.5	3.5	2.9
Small-signal gain α/cm^{-1}	0.228	0.220		0.075	0.05	0.0426
Stored energy/J	16	29		185	249	293
Number of passages	1	2		1	1	1
		1st passage	2nd passage			
Energy at amplifier output/J	0.8	2.5	10	36	66	110
ΔB increment	0.4	0.2	1.2	0.6	0.6	0.7
Total integral B_Σ	0.6	0.9	2.2	2.8	3.5	4.2

5. Transport telescopes

Transport telescopes (*14*), (*18*), and (*20*) are required to match the beam diameter with the amplifier apertures. In addition, they fulfil the function of repeaters (by lowering the intensity variations in AEs located in the conjugate planes of Keplerian telescopes [9, 24]), decrease the angle of vision of the amplifiers, and limit the high-frequency component of the spatial beam spectrum.

Constructively, the transport telescope is a metal cell evacuated to a pressure of 10^{-3} Torr. Lenses serves as the cell windows. To change the lens separation and thereby compensate for the quadratic component of wave-front distortions of the laser beams, the lenses are attached to the cell via flanges on flexible metal bellows. The lens diameters are 1.5–2 times greater than the beam diameter, and therefore mounting them by the edge using silastic does not introduce noticeable depolarisation into the laser beam. The lenses were made of K8 glass with the radii minimising the spherical aberration (Table 2). Both lens surfaces were covered with a stable antireflection coating.

At the centre of the cell an aperture was mounted on a miniature three-coordinate translatable stage, which could be displaced with the help of stepper motors with a minimal step of 6 μm along the optical axis and 2 μm transversely to it. The motors were remotely controlled with an analogue device or a computer.

Spherical aberrations. In the design of transport telescopes (*14*), (*18*), and (*20*) (Fig. 1), the spherical beam aberrations introduced by the telescope lenses should be taken into account. Neglecting diffraction, when a beam of radius R is incident on an infinitely thin lens (Fig. 9), all the rays parallel to the beam axis will pass through the focal point for an aberration-free lens [ray (*1*)]. Because of a spherical aberration, the rays will intersect the optical axis close to the focal plane for a focal distance $f > 0$ [ray (*3*)]. In this case, the intensity distribution in the focal plane spreads into a spot of radius r_s. The effect of spherical aberration can be estimated by comparing r_s with the diffraction-limited beam radius r_{dif}. When $r_{dif} \gg r_s$, the field distribution in the focal plane is little different from the far-field distribution pattern. Otherwise, the beam phase distortion arising from the spherical aberration in lenses has to be taken into account. For an infinitely thin spherical lens,

$$r_s = \frac{U}{f^2} R^3, \tag{3}$$

where

$$U = \left\{ \frac{n^2}{8(n-1)^2} - \frac{n}{8(n+2)} + \frac{1}{2n(n+2)} \left[\frac{n+2}{2(n-1)} \frac{1+C}{1-C} - n - 1 \right]^2 \right\}$$

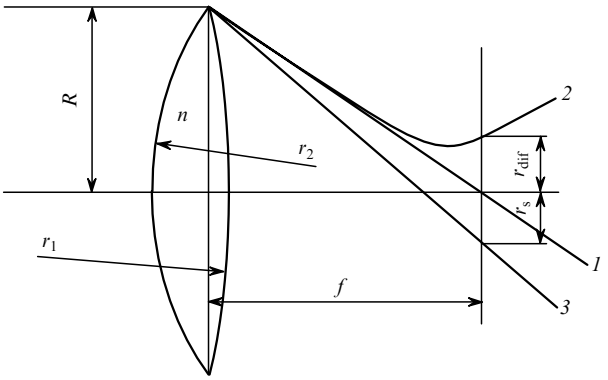

Figure 9. Ray paths in an infinitely thin lens.

is the Seidel parameter and $C = r_1/r_2$ is the ratio between the radii of curvature of the lens surfaces [25]. To every value of refractive index n there corresponds the optimal ratio

$$C_{min} = \frac{n(2n-1) - 4}{n(2n+1)},$$

for which U assumes the minimal value

$$U_{min} = \frac{n(4n-1)}{8(n+2)(n-1)^2}.$$

For instance, for $n = 1.5$, we have $C_{min} = -1/6$, and $U_{min} = 1.071$. With increasing n, C_{min} changes and U_{min} decreases. The parameters of the telescopes used in the setup are presented in Table 2. All the lenses were made of K8 glass; its refractive index at the laser wavelength $n_{1054} = 1.5063$, and $U_{min} = 1.053$. The radii of curvature obey the generally accepted sign rule: when a ray incident on the lens is parallel to the axis, for a convex lens $r_i > 0$ [25]. One can see from Table 2 that the ratios between the radii of curvature are close to the optimal value for all lenses, i.e. every lens makes the smallest spherical aberration possible for a single-component objective.

The diffraction-limited beam radius in the focal plane is

$$r_{dif} = \beta \frac{\lambda f}{2R}, \tag{4}$$

where $\beta = 1.22$ for a uniformly illuminated aperture and 1.7 for a plane wave transmitted through apodising screen (*8*) (Fig. 1). Taking (3) and (4) into account, the condition $r_{dif} \gg r_s$ limits the minimal focal lens distances:

$$f \gg \left(\frac{2UR^4}{\beta\lambda} \right)^{1/3}. \tag{5}$$

For instance, for a lens with minimal spherical aberrations ($U = 1.07$), for $\beta = 1.7$ and $R = 5$ cm we obtain

Table 2. Parameters of transport telescopes.

Telescope (label in Fig. 1)	Input lens				Output lens				Magnification	Aperture stop diameter/μm
	r_1/mm	r_2/mm	f/mm	U	r_1/mm	r_2/mm	f/mm	U		
(*14*)	436	−2500	734	1.053	1355	−6792	2233	1.056	3.04	1000
(*18*)	767	−4966	1314	1.053	1096	−6792	1866	1.053	1.42	1200
(*20*)	930	−4966	1548	1.054	1057	−6792	1808	1.053	1.17	1200

$f \gg 100$ cm, which is hard to realise if we set ourselves the task of accommodating the entire laser on a single optical table. However, due to the bell-shaped intensity distribution it is evident that the number of peripheral rays, i.e. the rays experiencing the maximum spherical aberration, is small. Figure 10 shows the far-field distribution pattern for a plane wave transmitted through the apodising screen, with neglect of and with the inclusion of aberrations introduced by the K8 glass lens with $f = 183$ cm and $C = -0.16$. One can see that even for $r_{\rm dif} \approx r_{\rm s}$ the inclusion of aberrations leads to only an insignificant increase in the field intensity away from the beam axis. Therefore, when estimating the intensity at the edge of the aperture placed in the focal plane of the Keplerian telescope, the intensity value obtained for the aberration-free lens can be used. Moreover, the stringent requirement (5) is alleviated and assumes the form

$$f > \left(\frac{2UR^4}{\beta\lambda}\right)^{1/3}.$$

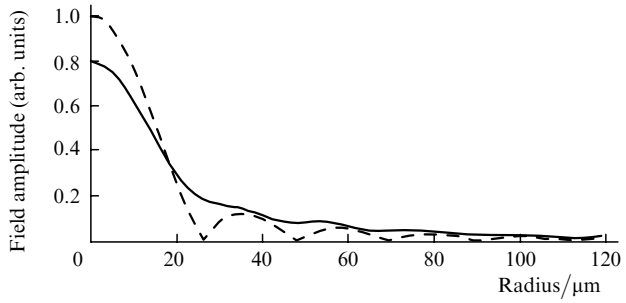

Figure 10. Radial dependence of the field amplitude in the focal plane of an infinitely thin lens formed by spherical surfaces with radii r_1 and r_2, for $f = 183$ cm and $r_1/r_2 = -0.16$, neglecting (dashed curve) and with the inclusion (solid curve) of spherical aberration. The near-field intensity distribution is defined by expression (1) with $r_{\rm d} = 4.9$ cm.

In a Keplerian telescope consisting of two confocal lenses, spherical aberrations manifest themselves in that a beam with an ideally plane wave front at its input will be distorted at its output. In this case, the rays passing through the input lens at a distance R_1 from the axis will converge to the axis at an angle $\Phi = (U_1/M + U_2)(R_1/f_1)^3$ at the telescope output, where $U_{1,2}$ and $f_{1,2}$ are the Seidel parameters and the focal distances of the telescope lenses and $M = f_2/f_1$ is the telescope magnification.

After sequential passage through telescopes (*14*), (*18*), and (*20*), the radiation divergence is approximately equal to the sum of divergences after passage of each individual telescope taking into account the magnification of the telescopes. A calculation of the inclination relative to the axis for a ray passing through the aperture edge showed that the spherical aberration deviates the ray by an angle $\Phi_0 = 60$ μrad upon sequential passage through these telescopes. A calculation of the far-field distribution with the inclusion of the phase arising from the total spherical aberration shows that the radiation divergence at the setup output amounts to three diffraction limits, i.e. to 40–55 μrad, depending on the filling factor. This means that there is no way of obtaining an output beam with diffraction-limited quality with the present facility dimensions unless special measures are taken to reduce spherical aberration (employing aspheric or multicomponent telescope objectives). At the same time, the 40–55 μrad divergence does not violate the requirement imposed on the divergence of laser radiation.

Spatial mode filtration and suppression of amplifier self-excitation. The overall small-signal gain G_0 of all stages exceeds 10^6 (see Table 1). In this connection there is a need to rule out the possibility of self-excitation and lower the energy of superluminescence, which is responsible for the inversion dumping in the AEs. To prevent self-excitation, Faraday isolator involving permanent magnets (*10*), (*11*) is introduced into the setup to ensure a 40 dB decoupling. Despite the antireflection coating, all laser elements are deflected off normal by an angle sufficient to remove the reflections from the amplifier aperture. The end faces of the AEs [excepting the AE of first amplifier (*9*), see Fig. 1] do not have antireflection coatings, and the reflections they produce propagate within a large angle. Their propagation is suppressed by apertures placed in the focal planes of transport telescopes (*14*), (*18*), and (*20*). The telescope thereby fulfil the function of spatial frequency filters (SFFs). In order that such filters do not distort the spatial beam structure, they should transmit a sufficiently broad angular spectrum. In this case, the higher aperture filling factor F, i.e. the closer the transverse beam distribution to the uniform one, the broader is the spatial spectrum to be transmitted by the SFF. For the SFF to introduce only an insignificant distortion into the transverse beam structure, the radius of the SFF aperture stop r_0 should satisfy the condition

$$r_0 > \frac{A\lambda f}{2R}, \tag{6}$$

where $A \simeq 1$ for small filling factors F [10], 10–20 for $F = 0.5 - 0.8$ [26], and ~ 60 for $F = 1$ [24].

By decreasing the angle of vision of the amplifiers, the SFFs not only reduce the probability that the reflections find their way into the amplifier apertures, but also reduce the power of superluminescence noise. For a four-level system, neglecting the radial dependence of the gain, the noise energy density $w_{\rm n}$ at the output of the amplifiers for $\ln G_0 \gg 1$ can be estimated by the formula [27]

$$w_{\rm n} = \frac{\hbar\omega_0 n^2 G_0 \Delta\omega \Delta\Omega \Delta t}{2\pi(\ln 2)\lambda^2 \ln G_0},$$

where ω_0 and $\Delta\omega$ are the central frequency and the width of Gaussian gain band; Δt is the inversion lifetime; $\Delta\Omega$ is the solid angle of vision of the amplifier ($\Delta\Omega \ll 1$). Therefore, by decreasing the solid angle with the help of a spatial filter, it is possible to efficiently reduce the power of the noise radiation component.

Without the use of spatial filtration, the angle of vision of the amplifiers is $\Delta\Omega = 2.9 \times 10^{-3}$ sr. For the highest gain $G_0 = 2.3 \times 10^6$, we obtain $w_{\rm n} = 0.32$ J cm^{-2}. This value, while lower than the saturation energy of neodymium phosphate glass of 3.5 J cm^{-2} [28], corresponds to a noise energy of 25 J at the output. With the employment of spatial filtration, the angle of vision of the amplifiers $\Delta\Omega$ was decreased down to nearly 1.26×10^{-7} sr without appreciable distortion of the beam structure. This had the effect that the noise energy density was lowered to a negligible value of 1.4×10^{-5} J cm^{-2}.

Suppression of small-scale self-focusing. Also among the

functions of transport telescopes is suppression of small-scale self-focusing (SSF) [18]. Qualitatively, the SSF is characterised by the buildup integral of small-scale perturbations – B-integral (2). It has been reliably determined that the buildup of small-scale noise in the transverse beam distribution will result in an optical breakdown when the increment of the B-integral over one amplifier stage is $\Delta B \geqslant 2-3$ [2, 3]. With reference to Table 1, in none of the amplifier stages does ΔB exceed unity. At the same time, the total integral $B_\Sigma = 4.2$, which may also lead to SSF. To avoid this, the transport telescopes should limit the high-frequency component of the spatial spectrum of the laser beams. The highest increment is inherent in the perturbations with the angular scale [18]

$$\Psi_{sf} = \left(\frac{8\pi n_2 I}{cn}\right)^{1/2}. \qquad (7)$$

For $n_2 = 1.17 \times 10^{-13}$ esu [19] and $I = 5$ GW cm^{-2} we have $\Psi_{sf} = 1.44 \times 10^{-3}$ rad. Therefore, an efficient suppression of an SSF will occur when an SFF transmits radiation in a solid angle with an opening angle of less than 1.44×10^{-3} rad. On the other hand, the SFF should possess a sufficiently large angle of vision so as not to distort the beam. From expressions (6) and (7) for $I = 5$ GW cm^{-2}, we obtain that efficient suppression of SSFs is possible only for a beam of radius $R \geqslant 1$ cm. In our case, however, the resultant increment $\Delta B = 2.2$ cm at the output of the second amplifier after the second passage through it (Table 1) does not result in the emergence of SSFs, because telescope (*14*) in the backward pass increases the scale three-fold and removes the resultant SSF from the path of highest gain increment.

6. Output parameters of the phosphate glass laser

Figure 11 shows a typical pattern of transverse intensity distribution in the plane of the output surface of amplifier (*21*) (Fig. 1) for a beam energy of 100 J and an aperture filling factor $F = 0.65$. In this case, $F = 0.4$ for the intensity distribution at the amplifier input (Fig. 7b). The far-field intensity distribution for the fundamental harmonic was obtained with the help of a two-component objective ($f = 300$ cm) corrected for spherical aberration. An analysis of this distribution showed that the difference between the distributions for low-energy pulses (1 – 10 mJ) and for 100-J pulses is insignificant. In this case, 50 % of the energy is contained in an angle of 30 μrad and 90 % in an angle of 90 μrad, which corresponds to 3 – 4 times the diffraction-limited divergence.

Despite the fact that the SSF is efficiently suppressed by the transport telescopes, the total B-integral is equal to 4.2 (see Table 1), which is indicative of some distortion of the beam phase, i.e. of the self-focusing of the beam as a whole. This will result in an additional beam divergence ϑ_{sf}. We estimate ϑ_{sf} employing the moments method [29]. To do this we approximate the radial intensity distribution of the laser beam with a super-Gaussian function $I(r) = I_0 \exp(-r^{2m}/w_0^{2m})$. By operating similarly to Ref. [30] it is possible to show that the expression for divergence at an e^{-1} beam intensity level is, after passage through a thin layer of a cubic nonlinear medium with a B-integral, of the form

$$\vartheta_{sf} = \frac{1}{kw_0}\left[\frac{m^2}{\Gamma(1/m)}\left(1+\frac{4}{9}B^2\right)\right]^{1/2},$$

where Γ is the gamma function. By taking advantage of the moments method it is possible to select a quadratic phase corrector which minimises the divergence:

$$\vartheta_{min}^2 = \frac{1}{(kw_0)^2}\left\{\frac{m^2}{\Gamma(1/m)} + \left[\frac{4}{9}\frac{m^2}{\Gamma(1/m)} - 2^{-2/m}\frac{\Gamma(1/m)}{\Gamma(2/m)}\right]B^2\right\}.$$

In our case ($w_0 = 3.68$ cm, $m = 3$, and $B = 4.2$), the beam divergence is $\vartheta_{sf} = 24.8$ μrad, which is 2.97 times the diffraction limit. By employing an $f = -1.22$ km lens it is possible to decrease the maximum divergence by a factor of two, i.e. to $\vartheta_{min} = 12.7$ μrad. To do this, the distance between the lenses of telescope (*20*) should be shortened to 2.7 mm. However, 'local' wave-front departures from planarity which make their appearance in the output laser beam because of imperfections of different optical elements exceed the focal distance of correcting lens. That is why the wave front distortions arising from the beam self-focusing for $B = 4.2$ have only a weak effect on its divergence.

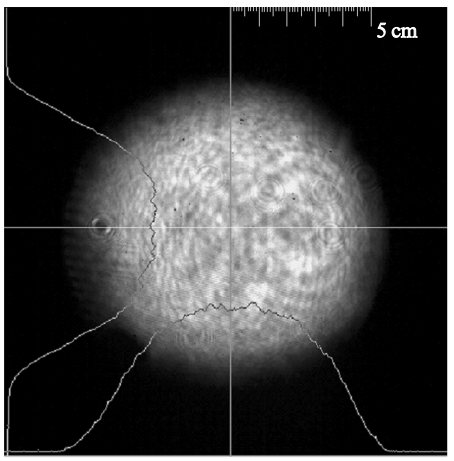

Figure 11. Transverse radiation intensity distribution at the setup output. The aperture filling factor is $F = 0.65$.

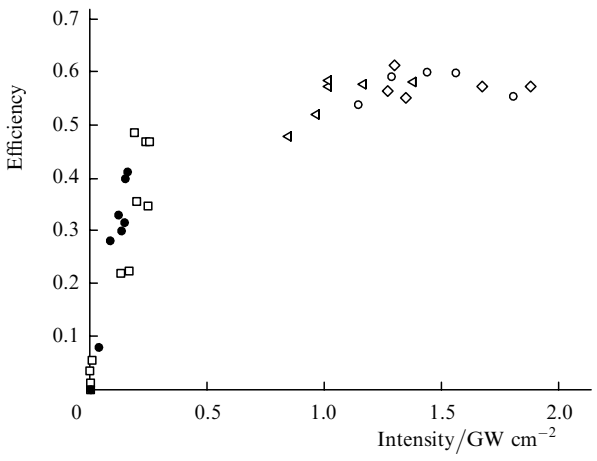

Figure 12. Efficiency of conversion of the output radiation to the second harmonic in a DKDP crystal. Points represent the experimental results on frequency doubling obtained in different series.

As a second harmonic generator we employed a 3.8-cm long DKDP crystal cut in the type-I phase-matching direction. The total phase-matching width for a weak signal was ±500 μrad [31, 32]. The accuracy of crystal axis alignment was equal to ±20 μrad. Figure 12 shows the energy efficiency of conversion of output laser radiation to the second harmonic as a function of intensity. In experiments we changed the aperture filling factor F of input amplifier stage (*9*) in the limits between 0.2 and 0.4. In this case, at the amplifier output $F = 0.5 - 0.65$. The maximum output intensity of the fundamental frequency radiation of 1.9 GW cm^{-2} was obtained for $F = 0.5$, while the highest energy equal to 110 J for $F = 0.65$.

7. Conclusions

A two-output system has been built for pumping an OPA of chirped light pulses. The first output permits obtaining 1.5-ns pulses with a repetition rate of 2 Hz, and an output energy of the second harmonic of 1 J. The second output delivers radiation pulses with a repetition period of 30 min, an energy of the fundamental harmonic up to 110 J, and the second harmonic energy up to 60 J. The radiation divergence at full power exceeds the diffraction limit by a factor of three. This divergence satisfies the requirement imposed on the pump radiation for an OPA based on a DKDP crystal 10 cm in diameter. Experiments with such an amplifier pumped by this system are currently underway. Their results will be reported in our next paper.

References

1. Andreev N.F., Bespalov V.I., Bredikhin V.I., Garanin S.G., Ginzburg V.N., Dvorkin K.L., Katin E.V., Korytin A.I., Lozhkarev V.V., Palashov O.V., Rukavishnikov N.N., Sergeev A.M., Sukharev S.A., Freidman G.I., Khazanov E.A., Yakovlev I.V. *Pis'ma Zh. Eksp. Teor. Fiz.*, **79**, 178 (2004).
2. Speck D.R. *IEEE J. Quantum Electron.*, **17**, 1599 (1981).
3. Bunkenderg J. *IEEE J. Quantum Electron.*, **17**, 1620 (1981).
4. Mak A.A., Lyubimov V.V., Serebryakov V.A., Fromzel' V.A., Yashin V.E. *Izv. Akad. Nauk SSSR. Ser. Fiz.*, **46**, 1858 (1982).
5. Alekseev V.N., Bordachev E.G., Borodin V.G., Gorokhov V.A., Kryzhanovskii V.I., Krylov V.N., Lyubimov V.V., Mak A.A., Migel' V.N., Malinov V.A., Nikotin V.V., Serebryakov V.A., Starikov A.D., Charukhchev A.V., Chernov V.N., Chertkov A.A., Yashin V.E. *Izv. Akad. Nauk SSSR. Ser. Fiz.*, **48**, 1477 (1984).
6. Bayanov V.I., Bordachev E.G., Kryzhanovskii V.I., Serebryakov V.A., Shchavelev O.S., Charukhchev A.V., Yashin V.E. *Kvantovaya Elektron.*, **11**, 310 (1984) [*Sov. J. Quantum Electron.*, **14**, 213 (1984)].
7. Bayanov V.I., Bordachev E.G., Volynkin V.M., Kryzhanovskii V.I., Mak A.A., Motorin I.V., Nikonova V.M., Serebryakov V.A., Starikov A.D., Charukhchev A.V., Shchavelev O.S., Yashin V.E. *Kvantovaya Elektron.*, **13**, 1891 (1986) [*Sov. J. Quantum Electron.*, **16**, 1240 (1986)].
8. Bayanov V.I., Vinokurov G.N., Zhilin V.I., Yashin V.E. *Kvantovaya Elektron.*, **16**, 253 (1989) [*Sov. J. Quantum Electron.*, **19**, 164 (1989)].
9. Kryzhanovskii V.I., Sedov B.M., Serebryakov V.A., Tsvetkov A.D., Yashin V.E. *Kvantovaya Elektron.*, **10**, 354 (1983) [*Sov. J. Quantum Electron.*, **13**, 194 (1983)].
10. Arifzhanov S.B., Ganeev R.A., Gulamov A.A., Redkorechev V.I., Usmanov T. *Kvantovaya Elektron.*, **8**, 1246 (1981) [*Sov. J. Quantum Electron.*, **11**, 745 (1981)].
11. Mustaev K.Sh., Serebryakov V.A., Yashin V.E. *Pis'ma Zh. Tekh. Fiz.*, **6**, 856 (1980).
12. Andreev N.F., Palashov O.V., Khazanov E.A. *Kvantovaya Elektron.*, **21**, 640 (1994) [*Quantum Electron.*, **24**, 588 (1994)].
13. Andreev N., Khazanov E., Palashov O. *Proc. SPIE Int. Soc. Opt. Eng.*, **3267**, 264 (1998).
14. Katin E.V., Lozhkarev V.V., Palashov O.V., Khazanov E.A. *Kvantovaya Elektron.*, **33**, 836 (2003) [*Quantum Electron.*, **33**, 836 (2003)].
15. Papernyi S.B., Serebryakov V.A., Yashin V.E. *Kvantovaya Elektron.*, **5**, 2059 (1978) [*Sov. J. Quantum Electron.*, **8**, 1165 (1978)].
16. D'yakova A.F., Kornev A.F., Reiterov V.M., Soms L.N., Stupnikov V.K., Tkachuk A.M., Ushakova O.A. *Izv. Akad. Nauk SSSR. Ser. Fiz.*, **55**, 294 (1991).
17. Bikmatov R.G., Boley C.D., Burdonsky I.N., Chernyak V.M., Fedorov A.V., Goltsov A.Y., Kondrashov V.N., Koptyaev S.N., Kovalsky N.G., Kuznetsov V.N., Milam D., Murray J., Pergament M.I., Petryakov V.M., Smirnov R.V., Sokolov V.I., Zhuzhukalo E.V. *Proc. SPIE Int. Soc. Opt. Eng.*, **3492**, 510 (1998).
18. Bespalov V.I., Talanov V.I. *Pis'ma Zh. Tekh. Fiz.*, **3**, 471 (1966).
19. Bondarenko N.G., Eremina I.V., Makarov A.I. *Kvantovaya Elektron.*, **5**, 841 (1978) [*Sov. J. Quantum Electron.*, **8**, 482 (1978)].
20. Malshakov A.N., Pasmanik G., Potemkin A.K. *Appl. Opt.*, **36**, 6403 (1997).
21. Frantz L.M., Nodvik J.S. *J. Appl. Phys.*, **34**, 2346 (1963).
22. Bespalov V.I., Pasmanik G.A. *Opticheskie Sistemy s Usilitelyami Yarkosti* (Optical Systems with Luminance Amplifiers) (Gor'kii: Izd. IPF AN SSSR, 1988) p. 39.
23. Martin W.E., Trenholme J.B., Linford G.J., Yarema S.M., Hurley C.A. *IEEE J. Quantum Electron.*, **17**, 1744 (1981).
24. Wegner P., Wonterghem B.V., Burkhart S., Widmayer C., Murray J. *LLNL. ICF Quarterly Report* (Livermore, Cal, 1999, Vol. 9, No. 1) pp 43 – 61.
25. Born M., Wolf E. *Principles of Optics* (Oxford: Pergamon Press, 1969).
26. Kuz'mina N.V., Rozanov N.N., Smirnov V.A. *Opt. Spektrosk.*, **51**, 509 (1981).
27. Makarov A.I., Potemkin A.K. *Kvantovaya Elektron.*, **12**, 1054 (1985) [*Sov. J. Quantum Electron.*, **15**, 692 (1985)].
28. Kryzhanovskii V.I., Serebryakov V.A., Yashin V.E. *Kvantovaya Elektron.*, **14**, 2407 (1987) [*Sov. J. Quantum Electron.*, **17**, 1531 (1987)].
29. Vlasov S.N., Petrishchev V.A., Talanov V.I. *Izv. Vyssh. Uchebn. Zaved., Radiofiz.*, **14**, 1353 (1971).
30. Makarov A.I., Potemkin A.K. *Izv. Vyssh. Uchebn. Zaved., Radiofiz.*, **30**, 1484 (1987).
31. Craxton R.S. *IEEE J. Quantum Electron.*, **17**, 1771 (1981).
32. Averbakh V.S., Makarov A.I., Potemkin A.K. *Kvantovaya Elektron.*, **11**, 2049 (1984) [*Sov. J. Quantum Electron.*, **14**, 1372 (1984)].